Retraction Phenomena of Surfactant Solution Drops upon Impact on a Solid Substrate of Low Surface Energy

Nadine Candoni, B Prunet-Foch, F Legay, M Vignes-Adler, K Wong

Langmuir **1999,** *15,* 6563−6574

Retraction Phenomena of Surfactant Solution Drops upon Impact on a Solid Substrate of Low Surface Energy

N. Mourougou-Candoni, B. Prunet-Foch, F. Legay, and M. Vignes-Adler*

Laboratoire des Phénomènes de Transport dans les Mélanges du CNRS 4 ter route des Gardes, F-92190 Meudon, France

K. Wong

Centre de Recherches d'Aubervilliers, Rhodia Recherche 52, rue de la Haie Coq, F-93308 Aubervilliers Cedex, France

Received February 2, 1999. In Final Form: May 7, 1999

The impact of surfactant solutions drop on a low-surface-energy solid substrate is investigated using a high-speed photographic technique (one picture every 100 μs) which allows simultaneous top and side views. The influence of physicochemical properties is analyzed by varying the adsorption kinetics of the surfactants and the initial diameter and velocity of the drop before impact. Generally, the drop spreads and retracts under the action of inertia and capillarity, respectively. During spreading, the drop shape changes from a "truncated sphere" to a "flat pancake" and the drop surface is increased such that it is no longer at thermodynamic equilibrium. The relevant surface property is therefore the dynamic surface tension which is evaluated at the maximum diameter $\gamma_{d_{max}}$, using the maximum bubble pressure apparatus. The dynamic surface tension has a critical influence on the drop behavior at the maximum diameter d_{max} and during the subsequent retraction. A simple relation combining $\gamma_{d_{max}}$ and the dynamic contact angle at d_{max} is derived to predict d_{max}. The results of this prediction agree well with the experimental measurements. Since $\gamma_{d_{max}}$ is large compared with the critical surface tension of the solid surface, a retraction of the drop is induced. The physical origin of this retraction is the apparent dynamic spreading coefficient S_{max} whose absolute value is correlated with the extent of the retraction. Two types of retraction are observed: a fast, destabilizing one which is described as an inertial peripheral dewetting and a slow, stabilizing one which relaxes exponentially. An empirical criterion is given on the basis of the difference between the thickness of the flattened drop at the maximum diameter and the critical thickness of metastability of a film in partial wetting conditions. It is demonstrated experimentally that this retraction proceeds on a clean solid surface and that the dewetted area is not modified by any surfactant adsorption which could have occurred during the contact time.

1. Introduction

Numerous industrial processes involve spreading of liquid drops due to impact on solid surfaces, for example, spray coating in painting and spray cooling in steel-making industries. In these applications, the maximum coverage of the target with the minimum amount of spray is desired. When drops produced from a spray nozzle reach the target surface, the coverage will depend on the manner in which the individual drops spread on the surface and coalesce together after impact. The behavior of a single drop upon impact on a solid is therefore a prerequisite piece of knowledge.

The typical behavior of a pure liquid drop colliding with a solid substrate can be described as follows: first, the drop spreads until it attains a maximum diameter, then it shrinks with or without an oscillating movement, and finally, it reaches equilibrium. Detailed studies of the impact process were initiated by Worthington[1] at the end of the last century. Much progress was made with the development of visualization technology[2] and computational methods. The spreading process was studied numerically first by Savic and Boult,[3] and then by Harlow and Shannon[4] who solved the Navier equation for the flow inside the drop neglecting the surface tension effects with a constant volume condition. Elegant experiments were performed by Chandra and Avedisian[5] on the collision of heptane drops with a stainless steel surface. Their experimental results compare fairly well with the Harlow and Shannon numerical predictions during the early stage of the spreading ($t < 500$ μs) when it is solely controlled by the inertial forces; this is the hydrodynamic stage of the impact. Moreover, energy conservation (including the surface energy term) of the drop before and after impact yields an expression of the maximum diameter attained by the flattened drop. However, the inferred value overestimated the diameter.

Actually, as the spreading velocity drastically decreases, the key properties are the capillary forces acting at the free surface and at the contact line between the drop and the solid surface. Recently, Fukai et al.[6] used a finite-element based method to integrate the complete Navier−Stokes equations of motion. They considered the normal and tangential stress balance conditions on the deforming free surface of the drop. Later, they accounted for the wetting effects by introducing advancing and receding static angles, before and after the maximum diameter,[7]

* To whom correspondence should be addressed.

(1) Worthington, A. M. *Proc. R. Soc. London* **1876**, *25*, 261.

(2) Edgerton, H. E.; Killian, J. R. *Flash! Seeing the Unseen by Ultra High-Speed Photography*; Hale, Cushman & Flint: Boston, 1939.

(3) Savic, P.; Boult, G. T. *Natl. Res. Counc. Can. Rep.* **1955**, No. MT-26.

(4) Harlow, F. H.; Shannon, J. P. *J. Appl. Phys.* **1967**, *38* (10), 3855.

(5) Chandra, S.; Avedisian, C. T., *Proc. R. Soc. London* **1991**, *A432*, 13.

(6) Fukai, J.; Zhao, Z.; Poulikakos, D.; Megaridis, C. M.; Miyataka, O. *Phys. Fluids* **1993**, *A5* (11), 2588.

(7) Fukai, J.; Shiiba, Y.; Yamamoto, T.; Miyatake, O.; Poulikakos, D.; Megaridis, C. M.; Zhao, Z. *Phys. Fluids* **1995**, *7* (2), 236.

respectively. Their theoretical model predicts fairly well the deformation of the impacting water drops, even during retraction and oscillation.

Now, all these works deal with pure liquids for which the surface tension remains equal to its equilibrium value whatever the deformation of the drop. Actually, just before impact, the droplet is fairly spherical and its surface tension can be considered as having its equilibrium value. Upon impact on the solid surface, the drop essentially becomes a pancakelike, and its total area is extended by 1 order of magnitude in a few milliseconds. Hence, if the liquid is not pure, the drop surface is no longer in thermodynamic equilibrium. At the maximum diameter, the surface tension increases due to the dilation of the surface and to the subsequent decrease of surfactant concentration at the free surface.[8,9] Few studies have been carried out with complex fluids such as surfactant solutions[8−10] and emulsions.[11,12] In the case of low concentration surfactant solutions, Pasandideh-Fard et al.[10] developed a numerical model in which they accounted for surface activity by introducing measured values of dynamic contact angles in the boundary conditions[13] and by assuming that the dynamic surface tension of surfactant solutions equals that of pure water. They also revised the Chandra and Avedisian model[5] to predict the maximum diameter by introducing the advancing contact angle in the expression of the surface energy and by improving the expression of the viscous dissipation in the energy balance. However, the models are solely valid for their particular dilute solutions since more concentrated solutions usually show dynamic surface tension effects.

In this context, Mourougou-Candoni et al.[9] have investigated the impact of drops of surfactant solutions with several adsorption kinetics; they have shown that for identical impact conditions the initial spreading due to the hydrodynamic effects follows the same "master curve" as pure liquids. They have also qualitatively demonstrated that the drop retraction is primarily influenced by the dynamic surface tension through the adsorption kinetics of the surfactants, which limits the restoration of the equilibrium surface tension. It will be shown here that the rate of surface dilational deformation influences the dynamic surface tension as much as the adsorption kinetics of surfactants. Finally, another surface property should be considered, namely, the surface energy of the solid substrate. Indeed, during drop spreading, as the solid surface is wetted by the liquid, its surface energy may be changed by some specific adsorption of surfactants. Hence, the retraction of the drops may occur on a modified surface.

The present paper is focused on the retraction phase. With a high-speed photographic technique allowing simultaneous top and side views, we investigate the influence of the physicochemical properties on the fate of surfactant solutions drops after impact. The dynamic surface tension is varied through both the adsorption kinetics of the surfactant and the rate of surface dilational deformation of the drop; the maximum diameter is evaluated by taking into account the corresponding dynamic surface tension and the dynamic contact angle. An apparent dynamic spreading coefficient is also defined at the maximum diameter and permits one to predict the retraction rate; a criterion for the occurrence of a rebound is discussed. The modification of the solid surface energy due to contact with the solutions is analyzed with ionic and nonionic surfactants.

Table 1. Properties of Liquids[a]

surfactants	cmc (g/L)	cmc × 10 γ_{lg} (mN/m)	cmc × 10 θ_e (deg)	cmc × 10 θ_a (deg)	cmc × 10 κ^{-1} (mm)
water		72.58	103	110	2.70
NPOEOP	0.06[a]	36.9	70	80	1.90
DOS	0.92[b]	27	∼10	22	1.64

[a] Measured with a Lecomte du Noüy-type tensiometer at 20 °C. [b] Literature value.[15]

2. Materials and Methods

2.1. Solid Substrate and Liquids. The solid substrate is a glass plate coated by complexed stearic acid; such a surface is smooth and hydrophobic with a critical surface tension approximately equal to 27 mN/m.

The liquids investigated are water and aqueous solutions of the nonionic surfactant nonylphenol polyoxyethylene (OE_{34}) polyoxypropylene (OP_{22}) (NPOEOP) and the anionic surfactant sodium dioctyl sulfosuccinate (DOS), both from Rhone-Poulenc. The experimental concentration of the surfactant solutions is 10 times the critical micellar concentration (cmc). For the sake of brevity, NPOEOP and DOS are used below instead of NPOEOP and DOS solutions at cmc × 10. For the preparation of the solutions, all of the dishes and instruments are carefully cleaned by degreasing with acetone and soaking in freshly made sulfochromic acid and then rinsed several times with pure water. The aqueous solutions of surfactants are prepared by weight and diluted if necessary to obtain the desired concentration. The shear dynamic viscosity μ is measured with a Contraves low shear viscometer at shear rates G of 1 and 10 s^{-1}. The values of μ are equal to (0.94 ± 0.02) mPas at 23 °C. The equilibrium surface tension γ_{lg} of the liquids is measured with a du Noüy-type apparatus using a stirrup instead of a ring, in a temperature-regulated cell set to 20 °C.[14] The equilibrium contact angle θ_e of a deposited drop on the substrate is determined with a G40 Krüss apparatus; the drop radius is smaller than the capillary length. The advancing contact angle θ_a is measured with a Wilhelmy plate apparatus. The values of cmc and of γ_{lg}, θ_e, and θ_a at cmc × 10 for these liquids are reported in Table 1.

Dynamic surface tensions γ_d are measured with a maximum bubble pressure method (MBPM) from Lauda, because the rates of surface dilational deformation obtained with this method are similar to the ones observed during the spreading process after impact.[9] This method is described in the Appendix. The γ_d values are plotted in Figure 1 as functions of surface lifetime τ for NPOEOP and DOS; the different rates of surface tension decay depend on the adsorption kinetics, which is faster for DOS than for NPOEOP. Since little data are available with MBPM at times shorter than 10 ms, the experimental data of γ_d are fitted and extrapolated to smaller times using the empirical equation deduced by Hua and Rosen[16] for ionic and nonionic surfactants (see Appendix).

The liquids are observed by fluorescence by means of a marker, the dextran fluorescein, which is introduced at a concentration of 5×10^{-5} mol/L. At this concentration, neither the surface tension nor the viscosity of the liquids are modified.

2.2. Experimental Procedure. A schematic representation of the experimental apparatus is shown in Figure 2. A similar apparatus for top views has already been described by Vignes-Adler et al.[11]; in this study, it has been improved to obtain simultaneous top and side views.

(8) Zhang, X.; Basaran, O. A. *J. Colloid Interface Sci.* **1997**, *187*, 166.
(9) Mourougou-Candoni, N.; Prunet-Foch, B.; Legay, F.; Vignes-Adler, M.; Wong, K. *J. Colloid Interface Sci.* **1997**, *192*, 129.
(10) Pasandideh-Fard, M.; Qiao, Y. M.; Chandra, S.; Mostaghimi, J. *Phys. Fluids* **1996**, *8* (3), 650.
(11) Vignes-Adler, M.; Legay-Désesquelles, F.; and Prunet-Foch, B.; *C. R. Acad. Sci. (Paris)* **1993**, *317* (II), 303.
(12) Prunet-Foch, B.; Legay, F.; Vignes-Adler, M.; Delmotte, C. *J. Colloid Interface Sci.* **1998**, *199*, 151.
(13) Dussan, V. E. B. *Annu. Rev. Fluid Mech.* **1979**, *11*, 371.
(14) Guastalla, J.; Lize, A.; Davion, N. *J. Chim. Phys.* **1971**, *68* (5), 822.
(15) Mukherjee, K.; Moulik, S. P.; Mukherjee, D. C. *Langmuir* **1993**, *9*, 1727.
(16) Hua, X. Y.; Rosen, M. J. *J. Colloid Interface Sci.* **1988**, *124* (2), 652.

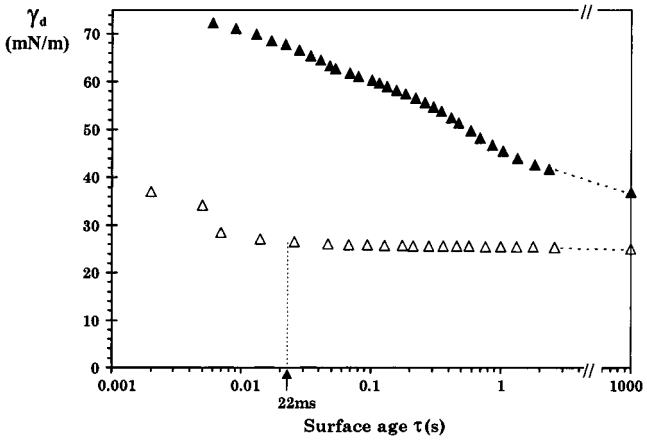

Figure 1. Dynamic surface tension γ_d as a function of the surface age for surfactant solutions at cmc × 10: ▲ NPOEOP and Δ DOS.

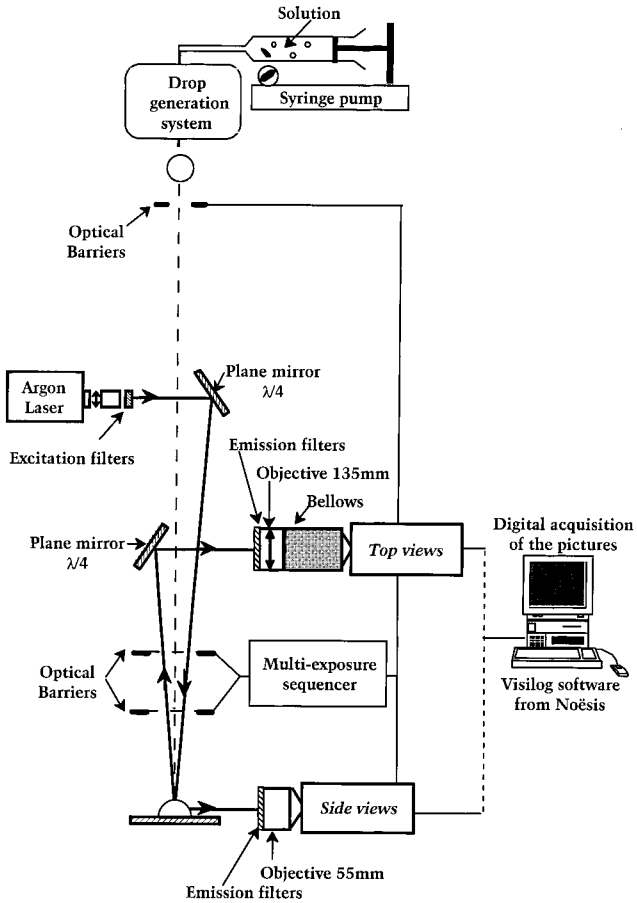

Figure 2. Experimental apparatus.

Drops are formed with two kinds of production systems in order to vary the rate of surface dilational deformation. "Large" drops (diameter of 2−3 mm) are formed at the tip of a capillary of outer diameter 0.67 mm and inner diameter 0.47 mm; they fall under gravity from a distance of 70 cm onto the solid substrate. "Small" drops (diameter of 700−900 μm) are generated with an apparatus using an air pulsed system[17] (Figure 3). The liquid flows through a capillary which is adjusted with four centering screws. Drops are formed at the end of a series of Teflon tubes with decreasing diameters, and they are blown off at the required diameter by an air flow pulse. The pulse is produced by opening a solenoid valve and the drop falling velocity is modulated by the air pressure. In this system, the drops are released from a height

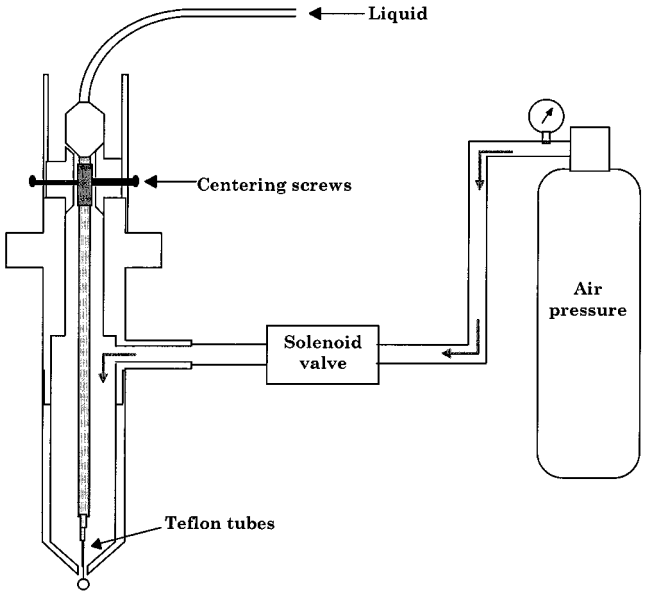

Figure 3. Air-pulsed system for the generation of small drops.

of 10 cm. The diameter and the velocity of drops are adjusted so as they fall vertically, and they collide as accurately as possible on the target at the center of the optical field. For both sizes of drops, impact velocity v_i and initial diameter d_i are summarized in Table 2. Note that whatever the liquid, the initial radii are smaller than the capillary length (Table 1) which compares the buoyancy to the capillary forces

$$\kappa^{-1} = \sqrt{\frac{\gamma_{1g}}{\rho g}} \tag{1}$$

where ρ is the density and g is the gravity acceleration.

The image acquisition system is composed of two high-definition cameras from Lhesa; the side view is provided by a tube camera with a light intensifier and the top view by a charge-coupled device intensified camera. Each camera is connected to a digitization card of 1024 × 1024 pixels^2 with 256 gray levels. The drops are observed by fluorescence by means of both a marker (dextran fluorescein) excited with an argon laser and appropriate filters. At the beginning of its fall, the drop is detected by the first optical barrier which sets to zero the clock of the cameras, and the shutter trigger. At the end of its fall, the drop passes through two other optical barriers which are connected to an electronic card; these interruptions trigger the electronic shutter of both cameras with a programmed shot delay (from −20 ms to 2 s), $t = 0$ s corresponding to the impact time. For every series, the exposure time (20 μs) and the gain of the cameras are adjusted to obtain the best contrast of the light intensity emitted by the marker. Drop photographs are processed with Visilog Software from Noësis.

With this high-speed photographic technique, one top view and one side view of the drop are simultaneously taken at a precise instant during the impact process. For the same initial conditions. (i.e., drop diameter, height of release, etc.), the impact phenomenon is sufficiently reproducible from drop to drop to reconstruct the drop dynamics with photographs of successive stages of the impact process as if the photographs were taken with a same drop. Besides, side views use a double-shot method; each photograph contains two superimposed exposures of the same drop. The delay separating these two exposures is fixed in such a way that the first corresponds to the drop in flight and the second corresponds to either the drop later in flight or the drop in spread on the solid surface. From the first kind of photographs, the average impact velocity v_i right above the surface can be deduced for each liquid; from the second kind, the moment of impact t_0 and the actual delay value t of the drop after impact can be calculated precisely with v_i. These side views also provide the initial diameter d_i and the dynamic contact angles θ of the splat. The precisions obtained with this procedure on d_i

Table 2. Drop Properties during the Spreading Process

liquids	d_i (mm)	v_i (m/s)	$\Delta A/A_{max}$	Δt (ms)	$\dot{\lambda}_{exp}$	$\gamma_{d_{max}}$ (mN/m)	$\theta_{a\,dmax}$ (deg)	$\beta_{max\,exp}$ (±0.15)	β^*_{max}	$\frac{\beta_{max\,exp}}{\beta^*_{max}}$	β^{PF}_{max}	$\frac{\beta_{max\,exp}}{\beta^{PF}_{max}}$
water	0.89	4.06	0.84	280	2990	72.58	110	3.39	3.57	0.95	3.57	
	2.75	3.51	0.90	2800	321			4.40	4.66	0.95	4.66	0.95
NPOEOP	0.70	4.81	0.84	220	3797	72.55	110	3.37	3.51	0.96	3.80	0.89
	2.50	3.20	0.89	2200	405	72.20	105	4.20	4.38	0.96	4.70	0.89
DOS	0.80	4.56	0.85	350	2440	60	100	3.60	3.67	0.98	3.99	0.90
	2.28	3.30	0.90	3500	256	39.70	85	4.35	4.59	0.95	4.77	0.91

and t_0 are about ±0.07 mm and ±30 μs, respectively. Eventually, top views give detailed information on the surface and the contact line of drops. In addition, the diameter of spread drop d is more precisely measured with top views thanks to the fluorescence of the liquids on the glass substrate.

3. Results

The behaviors of surfactant solutions and water drops have been observed from the moment of impact until 1 s after impact. Sequences of side and top views of small and large drops are shown in Figures 4a−c.

With water (Figure 4a) and NPOEOP (Figure 4b), the shape of the splat during the spreading process is the same for both sizes of drops, even if the maximum diameter is reached at 200−400 μs for small drops instead of 2−3 ms for large drops. (Note that the large drops images appear elliptical in Figure 4 due to the angle formed by the camera with the horizontal plane. This is only artifactual.) Side views show that the drops keep their spherical cap shape with a circular film developing at its periphery in the early stage of the spreading. Then, a peripheral rim appears and starts to thicken at the maximum diameter with weak azimuthal undulations (called festoons) at the drop periphery. These do not become fingers as is observed, for example, with water drops on steel plates.[12] With water, the number of festoons decreases during retraction, and their wavelength increases as in a reverse Rayleigh instability. Concentric capillary waves are also observed on the drop surface, particularly with small drops (at t = 1 ms). During retraction, they propagate toward the center of the drop in the flattened central zone. Then, these waves are amplified as the peripheral rim grows noticeably, and they produce a rebound that is the rise of a column of liquid. With water, this rebound is very large, and the liquid column become so unstable that drops separate from its top (at 4−5 ms with small drops and at 17−20 ms with large drops) as in a Rayleigh instability. Even if the capillary waves are less visible with NPOEOP, a rebound for both drop sizes is significant at 2−3 ms with small and 17−20 ms with large drops.

With DOS, small drops behave like water and NPOEOP drops. Retraction is accompanied by the propagation of a growing peripheral rim which collects the splat liquid. However, there is no rebound. With large drops, the rim diminishes and the retraction is smaller.

Then, whatever the liquid, the drops recover spherical shapes with different diameters and contact angles according to the liquid, and the equilibrium is attained at about 1 s.

A spreading factor β is defined in order to compare the different drop evolutions on the solid substrate

$$\beta = d/d_i \tag{2}$$

where d is the diameter of the wetted area and d_i is the initial diameter of the drop.

In addition, the time t is normalized by a characteristic time t^* depending on initial conditions, more precisely, on the initial radius r_i and the impact velocity v_i

$$t^* = \frac{tv_i}{r_i} \tag{3}$$

β is plotted in Figure 5 as a function of time t^* for water, NPOEOP, and DOS. The general aspect of the curves is identical whatever the drop size, and in the early stage of the spreading process, until $t^* < 1$, all of the experimental points fit a master curve. From $t^* = 1$ until the maximum spreading, β values are the lowest for the small drops. Eventually, the final β for water and NPOEOP are equal whatever the size, whereas small drops of DOS undergo higher retraction than large drops.

4. Discussion

The main points are the following ones. There is a huge rebound with water and a significant one with NPOEOP solutions for a same impact energy. In this latter case, it is remarkable that a rebound is observed despite the presence of surfactants which are known to damp capillary waves.[18] With DOS, a rim is obtained with small drops and it is damped with large drops.

The behavior of impacting drops results from the balance between inertia, capillary, and friction forces. First, drops spread beyond their equilibrium diameter due to the kinetic energy of impact. Thus, the triple contact line is submitted to a "back" force provoked by the departure from equilibrium, and therefore, it recoils. Before impact, the drop is spherical with a minimal surface, which is very close to the thermodynamic equilibrium. At the beginning of the impact, the drop crashes on the target rather than spreads on it, and the contact line is accelerated. Then, the shape of the drop changes from a "truncated sphere" with a surrounding film to a "pancake" (Figure 6); the motion of the liquid of the drop is submitted to an elongational axisymmetric flow near the stagnation point. When the drop approaches its maximum extension, the film displays a peripheral rim, which is purely a hydrodynamic effect.[6] The high dilation of the drop free surface generates an increase of its surface free energy which can be accounted for as $\Delta G^s = \gamma_{lg}\Delta A + A\Delta\gamma_{lg}$. For a surfactant-free liquid, ΔG^s reduces to $\gamma_{lg}\Delta A$. Since $\Delta A > 0$, the system therefore will naturally act to reduce or cancel this effect, unless the energy gain from covering the substrate dominates. The contribution of the change of surface tension to ΔG^s is more subtle and thus more difficult to analyze.

The characteristics of the free-deforming surface are severely modified by the elongational flow in the film, and these modifications can be described by four main features. (i) The elongational flow tends to induce surfactant accumulation toward the periphery of the free surface of the drop, decreasing locally the surface tension, and favors local surface deformation. (ii) The noticeable increase of the splat free surface including the rim free surface induces a dilution of the surfactants, which

(18) Levich, V. G. *Physicochemical Hydrodynamics*; Prentice Hall, Inc.: Englewood Cliffs, N.J. 1962.

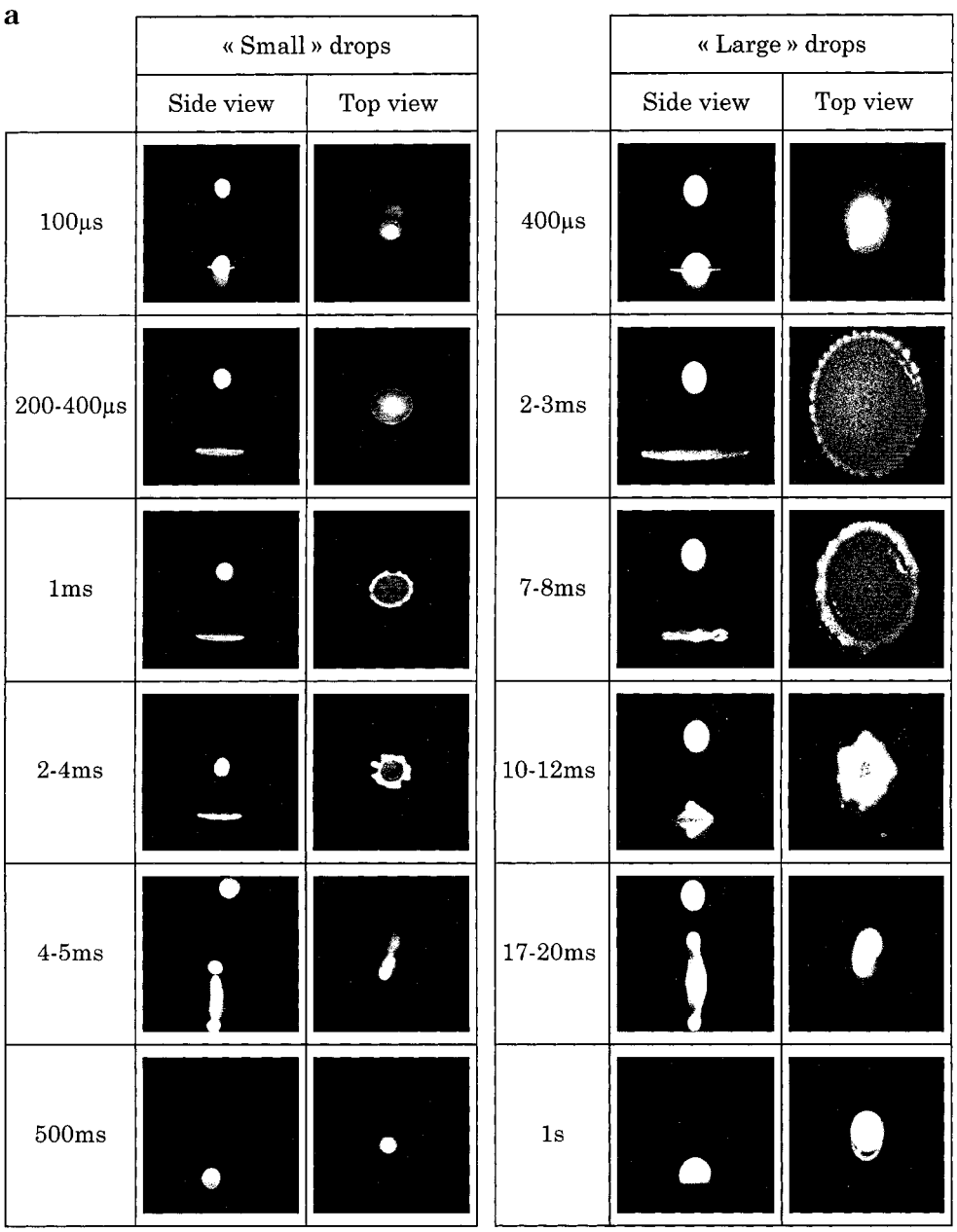

Figure 4a. Water drops. Sequence of side and top views obtained with both sizes of dops impacting a glass place coated by complexed stearic acid.

increases the surface tension and the dynamic surface tension effect and tends to weaken the previous effect. (iii) Now, all the surfactants being soluble in water, they tend to restore the surface equilibrium by matter transfer from the center of the film toward the surface with a kinetics which can be slow or fast. (iv) Eventually, surfactant adsorption from the bulk splat can occur during the spreading stage, modifying the substrate surface energy. The characteristic time scales of the adsorption kinetics of the surfactant at the splat free surface or at the substrate surface in contact with it are also to be compared to the experiment duration.

Both (i) the Marangoni counter flow effect due to the surface tension gradient and (ii) the dynamic surface tension effect are opposite to the spreading. The relative importance of effects i and ii was analyzed by Stone and Leal[19] in a numerical study on the influence of insoluble surfactants on deformation and splitting of a drop submitted to a stationary elongational flow; the elongational flow rejected the surfactants from the center of the free surface toward the periphery, and in their study, a uniform surfactant distribution was restored by surface diffusion. They have shown that for large elongational deformation rates with a good surfactant (large decrease of surface tension γ_{lg} with a small increase of adsorbed mass) the surface concentration gradient involved by the flow (effect i) remains very low due to high surface dilution (effect ii). Even if their physical situation is quite different, their conclusions can qualitatively be applied to the present study. Hence, at the maximum diameter, the dynamic surface tension is almost constant on the whole free surface of the drop and perhaps also on the rim. Then, effect iii, which leads to the restoration of equilibrium surface tension, is limited by the surfactant adsorption kinetics.

4.1. Surface Tension $\gamma_{d_{max}}$ and Dynamic Angle $\theta_{a\,d_{max}}$ at the Maximum Diameter. The dynamic surface tension at the maximum diameter $\gamma_{d_{max}}$ must be measured

(19) Stone, H. A.; Leal, L. G. *J. Fluid Mech.* **1990**, *220*, 161.

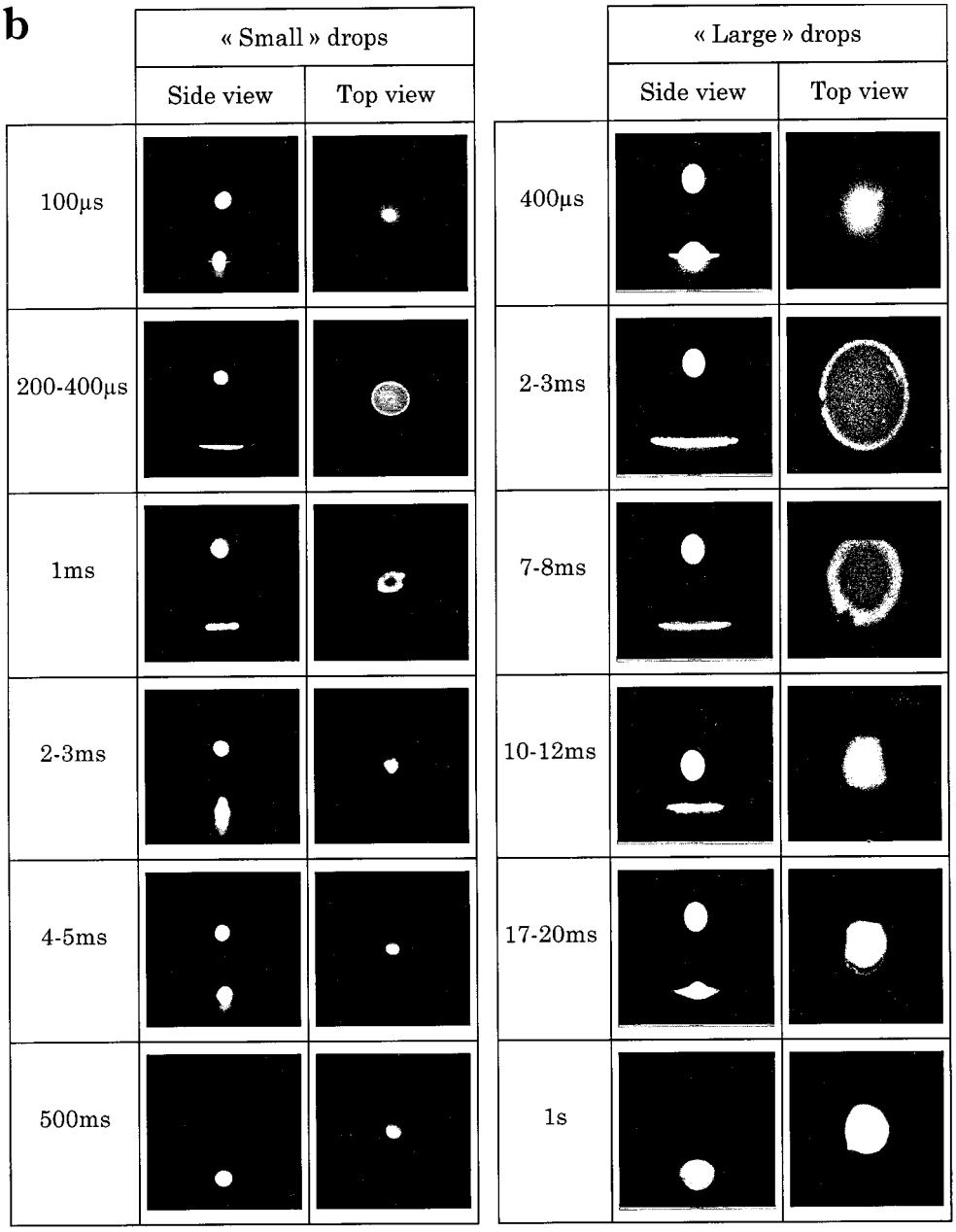

Figure 4b. NPOEPO solution drops. Same legend as Figure 4a.

in well-defined conditions. It depends on both the rate of dilational deformation of the free surface and the surfactant adsorption kinetics. $\gamma_{d_{max}}$ is equal to the measured dynamic surface tension γ_d for the same rate of surface dilational deformation as observed on the splat. At the moment of impact t_0, the drop has a spherical shape with a minimal total surface ($A_{min} = \pi d_i^2$). At the moment of the maximum extension t_{max}, the drop is assumed to be a flat pancake, and its surface A_{max} is calculated from the constant drop volume condition. Then, if during the spreading the surface extension rate is supposed constant, the experimental rate of surface dilational deformation can be defined by the relation

$$\dot{\lambda}_{exp} = \frac{\Delta A}{A_{max}} \frac{1}{\Delta t} \qquad (4)$$

where $\Delta A = A_{max} - A_{min}$ and $\Delta t = t_{max} - t_0$. Now, the MBPM gives γ_d as a function of surface age (Figure 1) or equivalently of the rate of surface dilational deformation $\dot{\lambda}_{th}$ when eq A.3 is used (see Appendix). In Figure 7, γ_d versus $\dot{\lambda}_{th}$ for DOS and NPOEOP are represented and $\gamma_{d_{max}}$ is obtained for $\dot{\lambda}_{th}$ equal to $\dot{\lambda}_{exp}$. For high $\dot{\lambda}_{exp}$, $\gamma_{d_{max}}$ is obtained by fitting the points with the Hua and Rosen approximation (eq A.2).[16]

The apparent dynamic contact angle θ_{dyn} at d_{max} depends on the velocity v_c and the direction of the contact line[13] as it is shown in Figure 8 in a spreading experiment of a deposited drop. In a complete wetting situation,[20] it verifies Tanner's law relating θ_{dyn} to v_c. In our experiments, it is very difficult to establish such a law due to the lack of accuracy on the evolution of θ_{dyn} with v_c during drop flattening. However, at d_{max}, the velocity v_c is low enough to measure the contact angle $\theta_{a\,dmax}$ on the photographs. For the case of pure liquids such as water, it is obvious from Figure 8 that $\theta_{a\,dmax}$ should be equal to the advancing contact angle θ_a.

The values of Δt, $\dot{\lambda}_{exp}$, $\gamma_{d_{max}}$, and $\theta_{a\,dmax}$ are reported in Table 2. Note that values of $\Delta A/A_{max}$ are the lowest for the

(20) de Gennes, P. G. *Rev. Mod. Phys.* **1985**, *57* (3), 827.

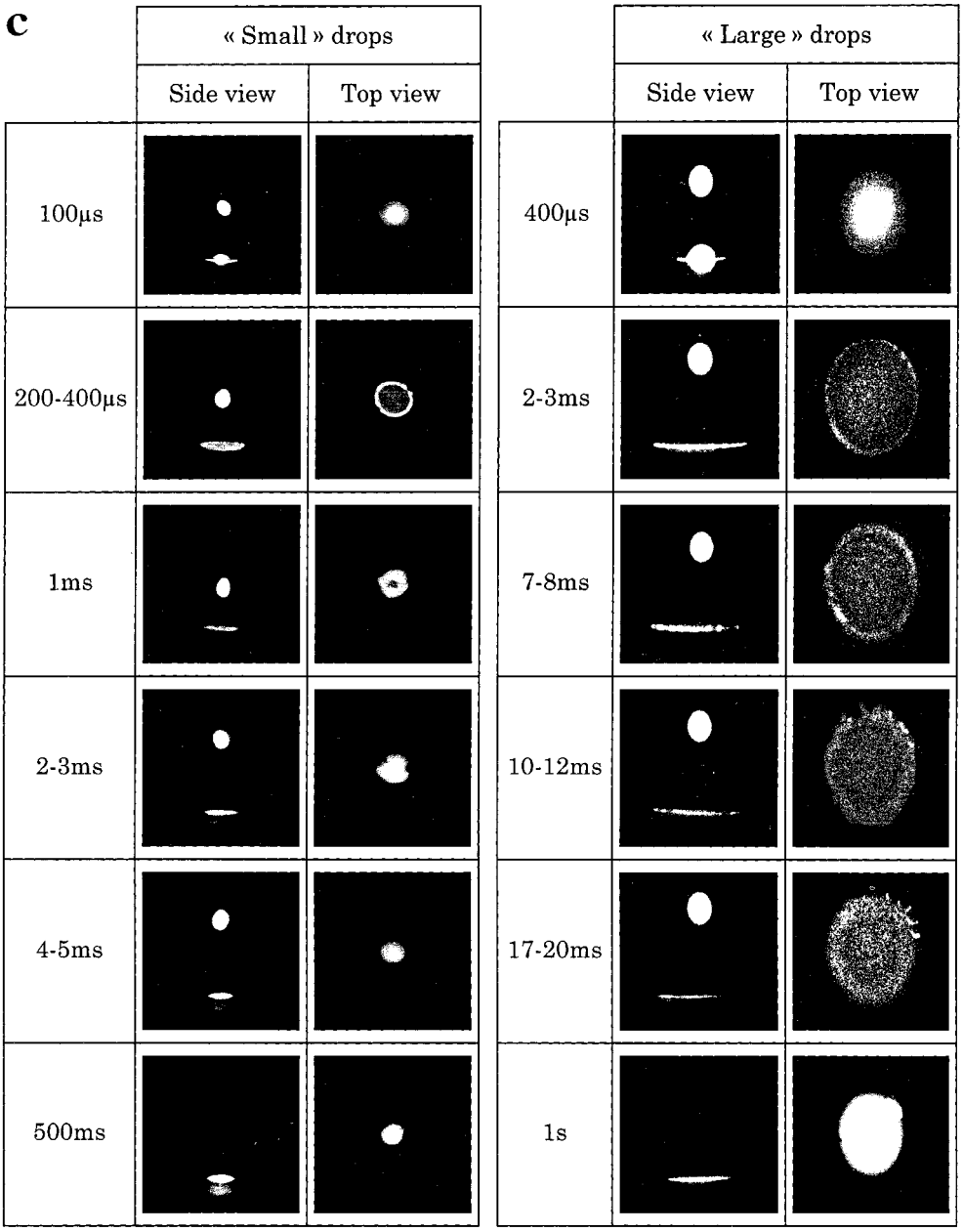

Figure 4c. DOS solution drops. Same legend as Figure 4a.

small drops due to the low kinetic energy. Δt is 10 times lower for small drops than for large ones and hence the opposite is true for $\dot{\lambda}_{exp}$. For small drops of DOS, this induces a higher $\gamma_{d_{max}}$, whereas for NPOEOP, the surfactant adsorption is so slow that $\gamma_{d_{max}}$ does not change with the present dilation rates. Moreover, $\gamma_{d_{max}}$ and $\theta_{a\ d_{max}}$ are related, and $\theta_{a\ d_{max}}$ is seemingly equal, within the experimental error, to the advancing contact angle of a liquid whose equilibrium surface tension would be equal to $\gamma_{d_{max}}$.

4.2. Maximum Diameter Calculation. The maximum diameter can be calculated using the energy conservation condition

$$E_{c1} + E_{s1} = E_{s2} + E_{diss} \tag{5}$$

E_{c1} and E_{s1} are the kinetic energy and the surface energy before impact

$$E_{c1} = \left(\frac{1}{2}\rho v_i^2\right)\left(\frac{\pi}{6}d_i^3\right) \tag{6}$$

$$E_{s1} = \pi d_i^2 \gamma_{1g} \tag{7}$$

E_{s2} is the surface energy at the maximum diameter d_{max}. The expression of E_{s2} derived here is an extension of that developed by Carey,[21] but the derivation accounts for the dynamic surface tension and contact angle

$$E_{s2} = (^1/_4\pi d_{max}^2)\gamma_{d\,max}(1 - \cos\theta_{a\ dmax}) \tag{8}$$

E_{diss} is the viscous dissipation in the peripheral rim. The present model is based on the work of Chandra and Avedisian[5] as revised by Pasandideh-Fard et al.[10]

$$E_{diss} = \int_0^{t_{max}} \int^V \phi \, dV \, dt \approx \phi V t_{max} \tag{9}$$

where ϕ is the viscous dissipation function. V is the volume of viscous fluid ($= {}^{\pi}/_4\ d_{max}^2\delta$), where δ is the thickness of

(21) Carey, V. P. *Liquid−Vapor Phase Change Phenomena*; Taylor & Francis: Bristol, PA, 1992; p 61.

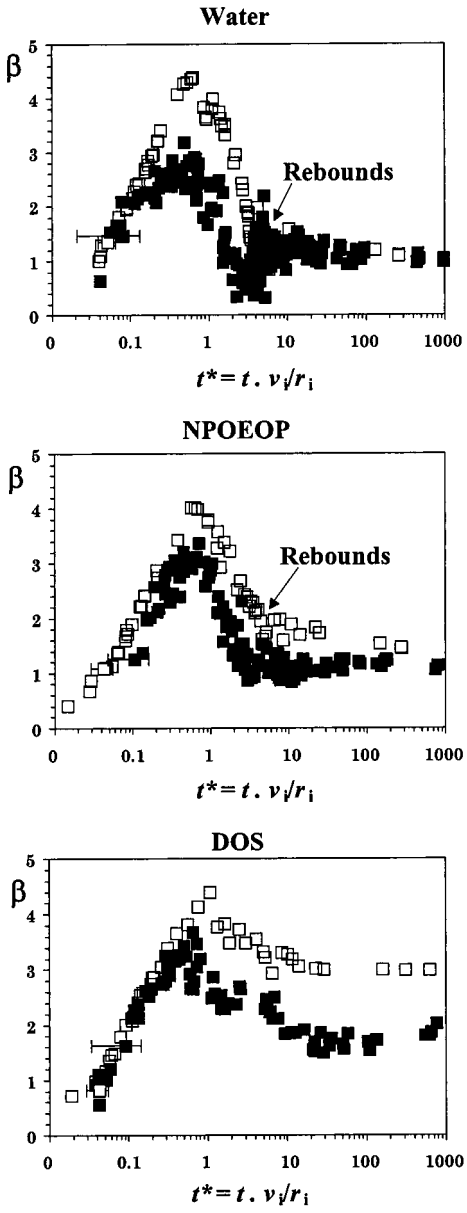

Figure 5. Spreading factor β versus nondimensional time t^* for water and NPOEOP and DOS solutions at cmc × 10: ■ small drops and □ large drops.

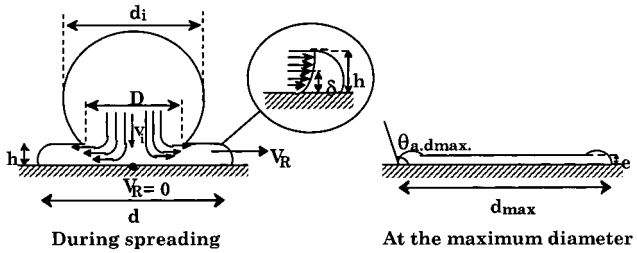

Figure 6. Shape of the drops during spreading and at the maximum diameter.

the viscous boundary layer (Figure 6). t_{max} is the time taken by the drop to reach the maximum diameter; it was derived by Pasandideh-Fard et al.[10] by assuming that the liquid flows from the drop shaped like a truncated sphere into a pancake at constant flow rate as $t_{max} = {}^{8}/_{3}(d_i/v_i)$.

Combining eqs 6−9 yields a relation between d_{max}, γ_{dmax}, $\theta_{a\,dmax}$, and γ_{lg}. Hence, an expression of the spreading factor is readily obtained introducing the Weber number (We = $\rho v_i^2 d_i/\gamma_{lg}$) and the Reynolds number (Re = $\rho v_i d_i/\mu$, with μ as the dynamic shear viscosity)

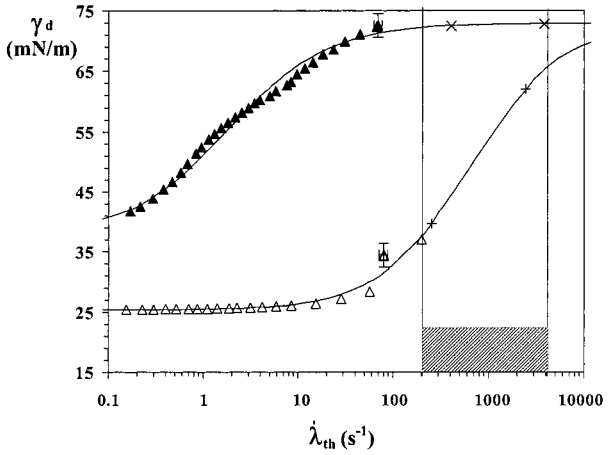

Figure 7. Dependence of the dynamic surface tension γ_d from the theoretical deformation rate in MBPM {[d(t) − d$_\infty$]/d$_\infty$} NPOEOP, and Δ DOS. Solid curves correspond to fit of γ_d with the equation of Hua and Rosen.[16]

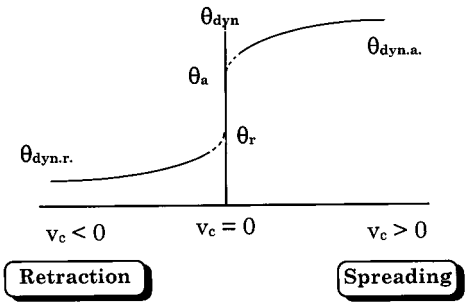

Figure 8. Apparent dynamic contact angle θ_{dyn} as a function of the contact line velocity v_c. θ_a and $\theta_{dyn\,a.}$: static and dynamic advancing contact angles. θ_r and $\theta_{dyn\,r.}$: static and dynamic receding contact angles.

$$\beta^*_{max} = \sqrt{\frac{We+12}{3\frac{\gamma_{dmax}}{\gamma_{1g}}(1-\cos\theta_{a\,dmax}) + 4\frac{We}{\sqrt{Re}}}} \qquad (10)$$

The values of β^*_{max} and the experimental values of $\beta_{max\,exp}$ are reported in Table 2. The present model is compared with the results of Pasandideh-Fard et al.,[10] who neglected the dynamic surface tension effects to derive the following:

$$\beta^{PF}_{max} = \sqrt{\frac{We+12}{3(1-\cos\theta_a) + 4(We/\sqrt{Re})}} \qquad (11)$$

Obviously, eqs 10 and 11 are identical for a surfactant-free water drop, and the inferred values compare well with $\beta_{max\,exp}$. However, eq 11 overestimates $\beta_{max\,exp}$ for surfactant solutions. In fact, $\gamma_{d_{max}}$ and $\theta_{a\,dmax}$ are very different from γ_{lg} and θ_a (Table 1), which allows eq 10 to be in very good agreement with $\beta_{max\,exp}$. Hence, it establishes that the maximum diameter dramatically depends on the dynamic surface tension effects.

4.3. Retraction. When drops are slowly deposited on a solid surface, a spreading coefficient S_{eq} defined by Harkins[22] is generally used to predict the drop evolution

(22) Ross, S.; Morrisson, I. D. *Colloidal Systems and Interfaces*; Wiley: New York, 1988.

Table 3. Drop Properties during the Retraction

liquids	d_i (mm)	S_{eq}	S_{max}	e_c (mm)	e (μm)	e/e_c	calculated v_d (cm/s)	measured v_d (cm/s)	θ_∞ (deg)
water	0.89	−89	−89	4.22	46	0.011			
	2.75	−89	−89		67	0.016	115	33	104
NPOEOP	0.70	−24	−60	2.18	31	0.014			
	2.50	−24	−60		86	0.039	83	29	69
DOS	0.80	0	−33	0.28	19	0.067			
	2.28	0	−13		80	0.29			11

$$S_{eq} = \gamma_{sg} - \gamma_{sl} - \gamma_{lg} \quad (12)$$

where γ_{sg} and γ_{sl} are, respectively, the solid−gas and solid−liquid interfacial energies. There is total or partial wetting if $S_{eq} \geq 0$ or $S_{eq} < 0$. Moreover, in partial-wetting conditions (finite contact angle θ_e) a film deposited on a solid substrate is metastable below a critical thickness e_c given by $e_c = 2\kappa^{-1} \sin(\theta_e/2)$.[20]

Now, in the present study, an apparent dynamic spreading coefficient S_{max} can similarly be defined when the drop reaches its maximum diameter. Since the surface of the drop is out of equilibrium, S_{max} depends on the dynamic surface tension $\gamma_{d_{max}}$

$$S_{max} = \gamma_{sg} - \gamma_{sl} - \gamma_{d_{max}} \quad (13)$$

Assuming that the retraction occurs on a clean solid surface (this hypothesis is discussed in section 4.4.) and introducing Young's equation ($\gamma_{sg} - \gamma_{sl} - \gamma_{lg} \cos \theta_e = 0$), eq 13 becomes

$$S_{max} = \gamma_{lg} \cos \theta_e - \gamma_{d_{max}} \quad (14)$$

S_{max} and S_{eq} are reported in Table 3. For surfactant solutions, S_{max}'s are always negative and strictly lower than S_{eq}. This explains why there is peripheral dewetting of the solid substrate and drop retraction. In the case of DOS, S_{max} is the lowest with small drops, and it corresponds to the highest retraction.

The thickness e of the flattened middle zone of the splat can be evaluated assuming that the rim is a half-torus whose chord is measured on the photographs and that the central zone is a disk. Then, e is obtained from the conservation of the drop volume before impact and at the maximum extension (Figure 6). Data reported in Table 3 show that e is lower than e_c so a metastability and a peripheral dewetting are occurring. For water, NPOEOP, and small drops of DOS, e is smaller than e_c by at least 1 order of magnitude. Hence, the splat is far from equilibrium, it becomes unstable, and strong retraction occurs with rebound for water and NPOEOP. For large drops of DOS, $e \leq e_c$, and the splat becomes stable. Hence, there exist two types of retraction: on one hand, high retraction with water, NPOEOP, and small drops of DOS and, on the other hand, low retraction with large drops of DOS.

High Retraction. The retraction is accompanied by the thickening of the peripheral rim which collects the liquid of the flattened middle zone. Moreover, converging capillary waves precede the rim (Figure 9) and finally a rebound is formed when the rim overpasses the capillary waves. The evolution of retraction $[d_{max} - d(t)]$ is plotted in Figure 10 as a function of the time gap $(t - t_{max})$ for large drops of water and NPOEOP. The results for small drops are not represented because the data are not sufficiently accurate. The contact line recoil proceeds at a constant velocity as long as the flattened middle zone is significant. Unfortunately, we could not measure the traveling velocity of the capillary waves.

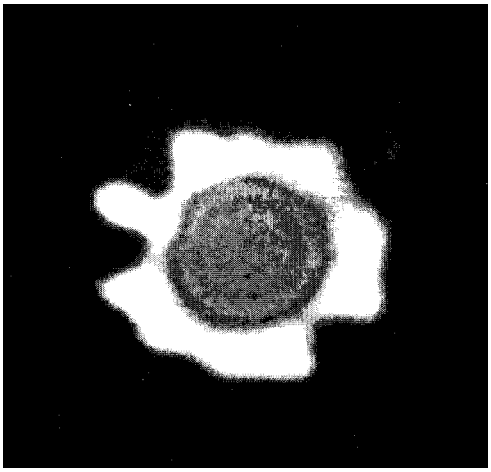

Figure 9. Enlarged top view of small drops of water at 3 ms.

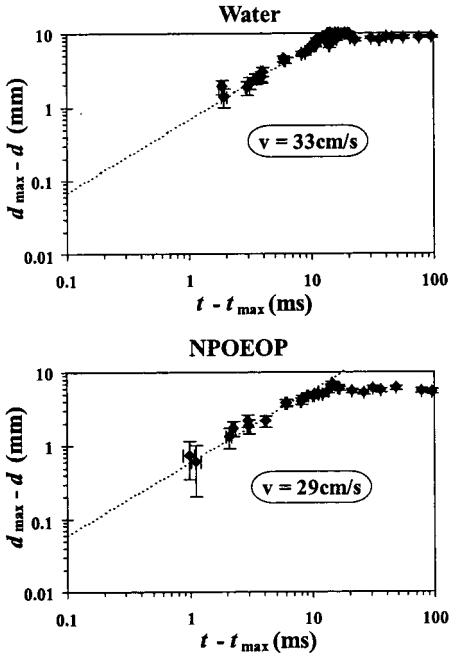

Figure 10. Evolution of the retraction $[d_{max} - d(t)]$ versus $(t - t_{max})$ for large drops of water and NPOEOP.

There is a complete analogy between the present experiment and the bursting of soap films[23−25] or of thick water films (500 μm) deposited on the same solid surface[26] except that (i) the geometrical configuration is the opposite and (ii) the film is not at rest at t_{max}. In both cases, the rim collects the liquid of the flattened middle zone which is shrinking at a constant thickness, according to the uniformity of gray levels observed on the photographs. In

(23) Ranz, W. E. *J. Appl. Phys.* **1959**, *30*, 1950.
(24) Lord Rayleigh *Proc. R. Inst.* **1891**, *13*, 261.
(25) Frankel, S.; Mysels, K. J. *J. Phys. Chem.* **1969**, *73*, 3028.
(26) Brochard, F.; Raphaël, E.; Vovelle, L. *C. R. Acad. Sci. (Paris)* **1995**, *321* (IIb), 367.

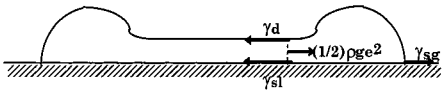

Figure 11. Forces balance during the retraction phase.

our experiment, the surface energy gained by the substrate dewetting is transformed into kinetic energy for the rim. The bursting velocity was calculated by Culick[27] for a foam liquid film of low viscosity and by Brochard et al.[26] for a dewetting film. The balance force can be written similarly except that the dynamic surface tension value should be used (Figure 11). Hence, the driving force of the retraction F_M per unit length of the contact line is given by

$$F_M = \gamma_d + \gamma_{sl} - \gamma_{sg} - (^1/_2)\rho g e^2 \qquad (15)$$

where the gravitational contribution ($1/2\rho g e^2$) is not neglected.

For water, γ_d is equal to the equilibrium tension. For surfactant solutions, as the rim keeps a large liquid−gas interface, we assume that γ_d remains close to the dynamic tension reached at the maximum diameter $\gamma_{d_{max}}$. Therefore, the surface tension terms in eq 15 can be replaced by the dynamic spreading coefficient S_{max} defined previously, and F_M is given by

$$F_M = -S_{max} - (^1/_2)\rho g e^2 \qquad (16)$$

The fundamental law of dynamics yields

$$\frac{d(m v_d)}{dt} = F_M \qquad (17)$$

where m is the rim mass.[26] The viscous dissipation can be neglected here because the solution viscosities are low and the rim is quite thick. Indeed, for a rim of 0.6 mm of thickness, the Reynolds number is equal to 200.

Then, we suppose that the variation of the rim inertia is essentially due to the increase of its mass at the expense of the central zone. Now, e is constant and the variation of the rim inertia is

$$\frac{d(m v_d)}{dt} = v_d \frac{dm}{dt} = v_d \rho e \frac{dr}{dt} = \rho e v_d^2 \qquad (18)$$

Combining eqs 16−18 gives the dewetting velocity v_d:

$$v_d = \sqrt{\frac{-\left(S_{max} + \frac{\rho g e^2}{2}\right)}{\rho e}} \qquad (19)$$

Calculated and measured values of v_d are reported in Table 3; eq 19 overestimates v_d by a factor of 3. A factor of 2 was generally observed in previous studies.[26] In the present case, the difference is increased by the divergent radial outflow inside the drop that goes on during retraction, after the maximum diameter.[6] It likely hinders considerably the recoil movement. Moreover, the viscous stresses are completely neglected in the model which is approximate in character. It is amazing that this over-simplified model works as well (or as bad!) for the water drops than for the NPOEOP ones. It is consistent with the very low adsorption kinetics of this surfactant and the increase of the surface rim during retraction. Usually, the surfactants can generate Marangoni stresses that damp the capillary waves and increase viscous dissipation.

(27) Culick, F. E. C. *J. Appl. Phys.* **1960**, *31*, 1128.

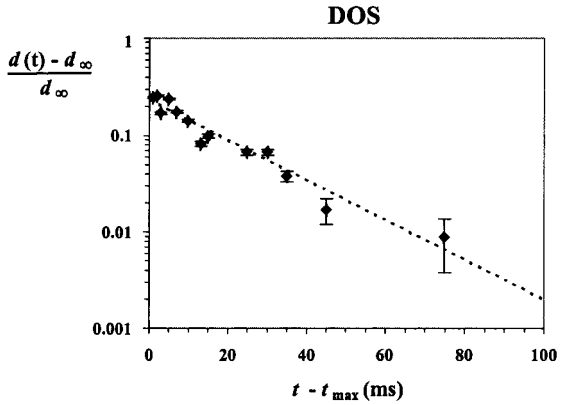

Figure 12. Evolution of $\{[d(t) - d_\infty]/d_\infty\}$ versus $(t - t_{max})$ for large drops of DOS.

Obviously, the presence of surfactants could not prevent the occurrence of converging capillary waves and the drop rebound; however, it lowered the rebound intensity.

Low Retraction. With large DOS drops, the thickness e is essentially on the same order of magnitude as e_c although almost 3 times larger. The retraction is low, the velocity is no constant, and the rim flattens (Figure 4c). In fact, at the maximum diameter, the drop is not far from equilibrium, and Figure 12 shows that it exponentially relaxes toward the final diameter d_∞

$$d = d_\infty(1 + e^{-t/T}) \qquad (20)$$

where $T_{DOS} \approx 22$ ms. Actually, this value is close to the characteristic time of the adsorption kinetics of DOS (Figure 1).

4.4. Influence of the Solid−Liquid Interactions. Just after the impact, the drops spread on a clean solid surface that they wet to the maximum diameter as long as they are in contact. During this spreading, surfactants can alter the solid surface properties by adsorbing on it. The contact angle θ_∞ reached at the equilibrium ($t = 1$ s) should therefore be different from the equilibrium contact angle θ_e of a deposited drop on a clean solid surface. The values of θ_∞ can be accurately determined by assuming that the drop shapes such as a spherical cap of diameter d, apex h, and volume Ω

$$\theta_\infty = 2 \arctan(2h/d) \qquad (21)$$

Equation 21 implies that at 1 s, capillary effects predominate because radii of the drops are smaller than the capillary lengths κ^{-1} of the solutions (Table 1). Then, straightforward geometrical considerations yield

$$\Omega = \pi h/6(3/2d^2 - h^2) \qquad (22)$$

$$\Omega = \frac{\pi d_i^3}{6} \qquad (23)$$

and h is readily obtained from eqs 22 and 23 as a function of d which is the more accurately measured quantity on the photographs.

The comparison of θ_∞ and θ_e (Tables 1 and 3) shows that they are equal within the experimental error. This means that the retraction proceeds on a solid surface whose energy has not been modified by the spreading of the drop. In fact, surfactants can adsorb on the surface only during the time elapsed between the impact and the beginning of retraction, in other words, approximately 10 ms, or less. Even if this time is sufficient for adsorption, with the

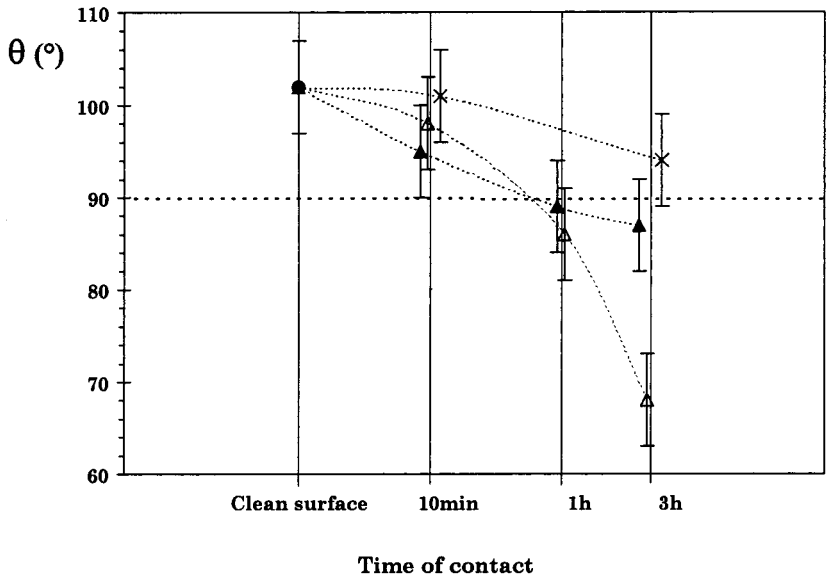

Figure 13. Evolution of the contact angle θ of a drop of water as a function of the time of contact between liquids and the substrate: ▲ NPOEOP, Δ DOS, and × water.

surface being hydrophobic, the surfactants adsorb by their hydrophobic tails via weak van der Waals forces, which may not be resistant to the flow and interface friction during the retraction step.

As far as we know, there is no direct experimental method which could measure adsorption resulting from a 10 ms contact time. We have therefore used two indirect methods. In the first one, we have compared the contact angle θ_0 obtained with a deposited drop of water on the clean solid surface to the θ measured on the same surface which has previously been wetted by NPOEOP or DOS during a given time (10 min and 1 and 3 h). The evolution of θ is plotted in Figure 13 as a function of the contact time between the surfactant solution and the surface. Up to 10 min, θ does not differ from θ_0 within experimental error. In addition, the values of θ are higher than 90° displaying hydrophobicity. Between 10 min and 3 h, θ decreases compared to θ_0. Besides, by performing the experiments on solid surfaces wetted by pure water over 10 min and 3 h, we verify that these effects are only caused by the surface-active solutes and not by water. These results can be compared to ellipsometric measurements of Tiberg[28] with a nonionic surfactant on a hydrophobic solid ($\gamma_c = 21$ mN/m); a maximal adsorption was obtained in less than 200 s, followed by a significant desorption. In our case, if surfactants have adsorbed at the solid surface, they should be removed in the bulk of the deposited drop of water, decreasing its surface tension and hence θ. However, an equilibrium must, at the very end, be achieved between the adsorbed and the bulk materials, and desorption cannot therefore be total. Moreover, this phenomenon should exist whatever the time of contact, whereas significant deviations of θ are only measured after a 30 min contact time.

The second method compares the advancing contact angles θ_a measured by the Wilhelmy plate method. These measurements are independent of a possible desorption of surfactants from the solid surface. We coated glass slides in the same manner as the solid surface that we plunged into a surfactant solution during a given time. Then, slides were dried in a U-nitrogen stream, and θ_a's were measured by immersion in pure water. The evolution of θ_a as a function of the contact time t with surfactant solutions is plotted in Figure 14. Until 10min, these angles are obviously close to those obtained with a clean surface within measuring errors (±5°). Thus, these results are consistent with the first results, and the adsorption is negligible for a contact time lower than 10 min. We also verified that wetting with pure water does not modify slides surfaces. In fact, the present solid surface possesses a low energy, and it is not easily polluted unless a chemical reaction, a dissolution of the stearic acid coating, or some penetration of surfactant molecules between the hydrocarbon chains, or so on occurs.

5. Conclusion

We have investigated the forced spreading of a drop which partially wets a solid substrate. When the drop impacts on the solid, it spreads further than its equilibrium diameter because of its initial kinetic energy. Then, it retracts under the action of the capillary forces acting at its free surface. The very early stage of the spreading is solely controlled by the inertial forces and is independent of the nature of the drop liquid and of the physicochemical forces. However, during its very fast spreading and flattening, the drop experiences such a large dilation rate of its free surface that, for surfactant solutions, it is completely out of equilibrium when it reaches its maximum diameter. The relevant surface property is now the dynamic surface tension which is always higher than the equilibrium value. It depends not only on the adsorption kinetics of surfactant but also on the rate of dilational deformation of the free surface which varies with the impact kinematic conditions.

The main results on retraction can be summarized as follows:

(i) The thermodynamic equilibrium surface tension of the liquid cannot be used to predict the maximum diameter attained by the drop upon impact. There exists a simple relationship between the maximum diameter, the dynamic surface tension, and the dynamic contact angle at the maximum diameter.

(ii) A dynamic spreading coefficient S_{max} can be defined and measured at the maximum diameter. For the surfactant solutions, S_{max} is always negative and $|S_{max}|$ is higher than the equilibrium value. It explains why retraction occurs and can be seen as a peripheral dewetting.

(28) Tiberg, F. *J. Chem. Soc., Faraday Trans.* **1996**, *92* (4), 531.

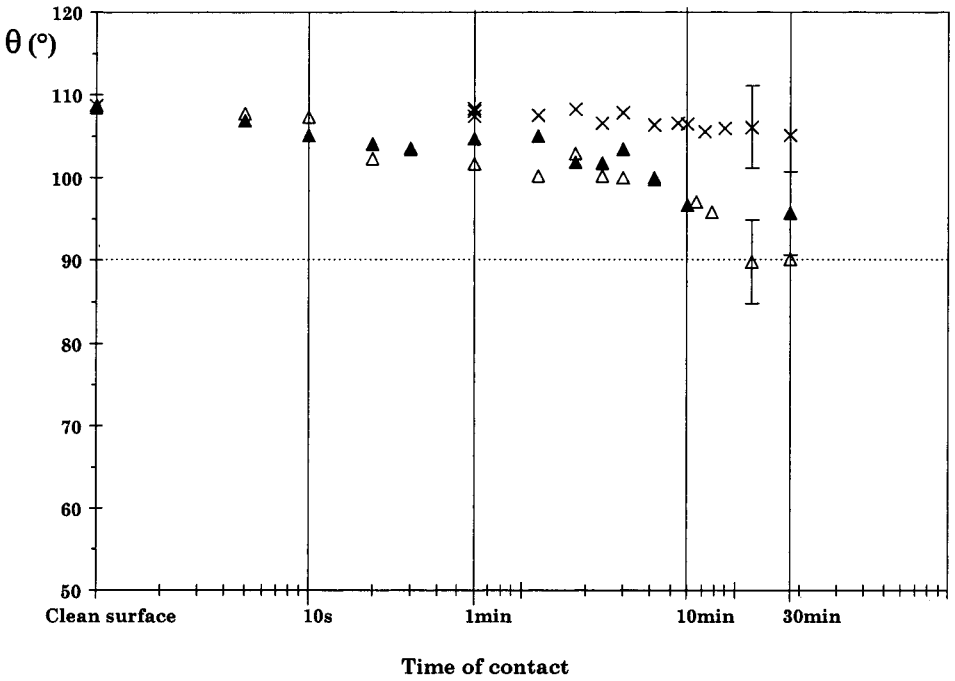

Figure 14. Evolution of the advancing contact angle θ_a of a drop of water as a function of the time of contact between liquids and the substrate: ▲ NPOEOP, Δ DOS, and × water.

(iii) Two types of retraction have been observed, depending on the deviation of the splat thickness e at the maximum diameter from the critical thickness e_c of metastability of a film in partial wetting conditions. If $e \ll e_c$, the retraction occurs at constant recoil velocity as in the rupturing of foam films; it is destabilizing for the film and a rebound of the drop can be observed. Hence, the comparison of e and e_c is a good criterion for drop rebound. If $e \approx e_c$, there is an exponential relaxation of the drop toward its equilibrium position.

Acknowledgment. N. M.-C. thanks Rhone-Poulenc for a doctoral fellowship.

Appendix

The maximum bubble pressure method (MBPM) consists of creating a bubble at the end of a fine capillary that is immersed at a depth h under the surface of a solution.[29] The pressure P inside the growing bubble is related to the γ_d and the radius R of the bubble by the Laplace equation (eq A.1), after correcting for the hydrostatic pressure ($p = \rho g h$) at the tip of the capillary

$$P = \frac{2\gamma_d}{R} + \rho g h \qquad \text{(A.1)}$$

When the pressure reaches its maximum value P_{max}, the bubble being hemispheric, the radius R is the same as the known radius r of the capillary and γ_d can be calculated. The MBPM measures the time interval τ_b between subsequent bubbles through the bubble frequency, whereas the time corresponding to γ_d is the surface lifetime τ of the hemispherical bubble. Austin[30] established specifically that τ_b includes τ and the so-called "dead time". Then, Kloubek[31] derived a simple experimental procedure for the determination of the dead time. In the setup that we have used, available as the commercial device MPT1 from Lauda (Germany), all the theoretical and experimental problems are assumed to be solved.[32]

As few data are available with MBPM at times shorter than 10 ms, the experimental data of γ_d can be fitted and extrapolated to smaller times using the empirical equation deduced by Hua and Rosen[16] for ionic and nonionic surfactants. At constant surfactant concentration in the bulk and constant temperature, they reported that γ_d is very well described by the equation

$$\gamma_d = \gamma_m + \frac{\gamma_o - \gamma_m}{1 + \left(\frac{\tau}{t'}\right)^n} \qquad \text{(A.2)}$$

The parameters t' and n are empirical constants evaluated for each surfactant solution, γ_d is the surface tension at surface age τ, γ_m is the meso-equilibrium surface tension, and γ_0 is the equilibrium surface tension of the pure solvent.[16]

In the MBPM, the rate of bubble surface dilational deformation $\dot{\lambda}_{th}$ is determined using the initial and final values of the bubble surface area approximated by Fainerman,[33] $A_{min} = 2\pi r^2/(1 + \sin \phi_0)$ and $A_{max} = 2\pi r^2$, where ϕ_0 is the initial boundary wetting angle of the capillary. Then, $\dot{\lambda}_{th}$ is related to the surface age τ

$$\dot{\lambda}_{th} = \frac{\sin\phi_0}{1 + \sin\phi_0}\tau^{-1} = \xi\tau^{-1} \qquad \text{(A.3)}$$

The surface dilational deformation ξ is weakly dependent on γ_d and is approximately equal to 0.4.[33]

LA9901074

(29) Miller, R.; Dukhin, S. S.; Kretzschmar, G. *Dynamics of Adsorption at Liquid Interfaces, Studies in Interface Science* **1995**, 1.
(30) Austin, M.; Bright, B. B.; Simpson, E. A. *J. Colloid Interface Sci.* **1967**, *23*, 108.
(31) Kloubek, J. *J. Colloid Interface Sci.* **1972**, *41*, 1−7.
(32) Fainerman, V. B.; Makievski, A. V.; Miller, R. *Colloids Surf. A* **1993**, *75*, 229.
(33) Fainerman, V. B. *Colloids Surf.* **1992**, *62*, 333.